Weld Pool Development during GTA and Laser Beam Welding of Type 304 Stainless Steel, Part I—Theoretical Analysis

The analysis reveals the realistic influence of surface active elements and temperature distribution on penetration

BY T. ZACHARIA, S. A. DAVID, J. M. VITEK AND T. DEBROY

ABSTRACT. A computational and experimental study was carried out to quantitatively understand the influence of the heat flow and the fluid flow in the transient development of the weld pool during gas tungsten arc (GTA) and laser beam welding of Type 304 stainless steel. Stationary gas tungsten arc and laser beam welds were made on two heats of Type 304 austenitic stainless steels containing 90 ppm sulfur and 240 ppm sulfur. A transient heat transfer model was utilized to simulate the heat flow and fluid flow in the weld pool. The current investigation differs from earlier modeling studies which assumed a constant temperature coefficient of surface tension $\frac{d\gamma}{dT}$ at the weld pool surface independent of both the local temperatures and the concentration of surface active elements such as sulfur. In the present investigation, $\frac{d\gamma}{dT}$ was calculated as a function of temperature and sulfur content. This allows for a realistic simulation of the effect of the concentration of surface active elements on the fluid flow and weld geometry.

Here, in Part I of the paper, the results of the heat flow and fluid flow analysis are presented. In the accompanying Part II, the calculated results are compared with the results of the experimental investigation. It has been shown that the spatial variation of surface tension that exist on the weld pool surface dominates the fluid flow and controls the development of the weld pool for both welding processes. Increasing the sulfur content increased the weld penetration during GTA welding. During laser beam welding, the increased sulfur content did not have an appreciable effect on the weld pool size or shape. It has been shown that the weld penetration and the aspect ratio are not determined solely on the basis of the level of the surface active elements in the base metal but rather due to a combination of the level of surface active elements and the temperature distribution at the weld pool surface. Good agreement was found between the predictions of the model and experimental observations with respect to fusion zone size and shape as shown in Part II, thereby verifying the predictions of the computational model employed.

T. ZACHARIA, S. A. DAVID and J. M. VITEK are with the Metals and Ceramics Div., Oak Ridge National Laboratory, Oak Ridge, Tenn. T. DEBROY is with the Dept. of Materials Science and Engineering, Pennsylvania State University, University Park, Pa.

Introduction

It is well known that the heat transfer experienced by the weldment during welding can alter the microstructure and thus the properties of the weldment. The heat flow and the fluid flow in the weld pool can significantly influence the pool geometry, the temperature gradients, the local cooling rates and the solidification structure (Refs. 1, 2). Experimental determination of the temperature distribution and cooling rates in a weldment during and after welding is extremely difficult. Therefore, in recent years, there has been considerable interest in quantitatively determining the detailed temperature and flow conditions that occur during welding by mathematically modeling the physical phenomena that occur (Refs. 3–11). Prior modeling efforts have addressed specific welding conditions and processes. Very little work has been done to compare, for the same material, the effect of welding process on the evolution of weld pool geometry and solidification structure. Such comparisons can yield valuable information about individual processes and provide an opportunity for understanding an individual effect such as electromagnetic force.

KEY WORDS

Modeling of Welding
GTA Welds
Laser Beam Welds
Stationary Welds
Linear Welds
Electromagnetic Force
Surface Tension
Minor Elements
Flow Field
Temperature Field

The dynamics of heat flow and fluid flow in the pool and their influence on the solidification structure are vastly different for different welding processes. During laser beam welding, the base metal is irradiated with a high energy beam causing rapid melting and solidification. Due to the large temperature gradient on the surface of the weld pool, there exists a significant surface tension gradient, which is the dominant driving force for fluid flow in the molten pool. On the other hand, during gas tungsten arc (GTA) welding, an electric arc is struck between the electrode and the workpiece. The resulting melting and solidification rates are lower. During GTA welding, in addition to the surface tension force, an electromagnetic force is generated due to the interaction between the welding current and the self-induced magnetic field. Depending on the temperature coefficient of the surface tension $\left(\frac{d\gamma}{dT}\right)$, flow due to the electromagnetic force may augment or counteract the surface tension gradient driven flow. The direction and magnitude of the fluid flow, in turn, affect the temperature field and the cooling rates at every location in the weld, and thereby influence the final weld metal solidification structure.

Recent studies (Refs. 1–11) have demonstrated that, in most cases, the fluid flow and the heat transfer in the weld pool

are controlled by the spatial variation of surface tension (surface tension gradient) that exists on the weld pool surface. The spatial variation of surface tension causes the molten metal to be drawn along the surface from the region of lower surface tension to that of higher surface tension, and this may result in very large surface flows. For pure metals and alloys $\frac{d\gamma}{dT}$ is negative. Thus, the surface tension is highest near the solid-liquid interface (lower temperature) causing the flow to be outward and away from the center of the pool. However, surface active elements, such as sulfur or oxygen, can produce a positive $\frac{d\gamma}{dT}$ resulting in a higher surface tension at the center of the pool, causing an inward flow. The effect of surface active elements has been investigated in detail by Heiple, *et al.* (Refs. 1, 12–14). His results indicate that surface active elements significantly alter the surface tension of the weld metal, thereby altering the flow field in the weld pool. Of particular significance is the reversal of flow that can occur in the presence of relatively small amounts of surface active elements, causing a deeper penetration. Sundell, *et al.* (Ref. 9), has experimentally investigated the effect of sulfur, silicon, cerium, oxygen and nitrogen on GTA weld penetration. His results indicate these elements can directly or indirectly influence the weld pool shape and size.

Most investigations of the effect of surface active elements on weld penetration have been carried out for GTA welding of steels. While the effect has been identified, the extent and the nature of the influence of surface active elements on weld pool fluid flow and depth of penetration remain to be clarified. A quantitative understanding of the effect of surface active elements on weld pool fluid flow and fusion zone shape can be achieved by mathematical modeling. Prior modeling efforts (Refs. 3–11) aimed at understanding surface tension gradient driven flow in the presence of surface active elements considered a specified constant positive $\frac{d\gamma}{dT}$, which cannot be justified based on the physical phenomena governing the process. Therefore, in the present analysis, a more realistic procedure (Ref. 16) that involves calculation of the surface tension as a function of the surface temperature and the amount of surface active element in the melt was utilized.

Parts I and II of the study present the results of a theoretical and experimental investigation aimed at understanding the effect of welding processes, namely GTA and laser beam welding processes, and surface active elements on the evolution of weld pool shape, size and the solidification structure. Stationary welds were made using conventional GTA and laser beam welding processes on the same material for different durations to provide a variety of solidification conditions, such as cooling rates and temperature gradients. The computational model was used to simulate the fluid flow, temperature distributions, local cooling rates and the weld pool shape and size. The model incorporates a recently developed formalism (Ref. 16) that calculates the surface tension as a function of temperature and the amount of surface active elements in the base metal. The time evolution of the weld was modeled for both GTA and laser beam welding conditions, and the results were compared with experimental observations of the weld. The computational model and the simulated results are presented in Part I. The results of the experimental investigation and comparisons with the theoretical results are presented in Part II.

Theoretical Investigation

The development of the weld pool is influenced by the simultaneous occurrence of several important physical processes. These include the amount of heat transferred from the heat source to the workpiece, the fluid flow in the weld pool, and the accompanying convective heat transfer. The amount of heat absorbed by a material is substantially different for the two welding processes examined. For the GTA welding process, a wide range of arc efficiency values, 21 to 93%, have been reported in the open literature (Refs. 17–20). Recently, Smartt, *et al.* (Ref. 20), measured the amount of energy absorbed by the workpiece using dry calorimetry. In this technique, the total heat content in the workpiece is determined by measuring the change in mass due to boiling of a given volume of liquid nitrogen. Arc efficiency was found to be 75%. However, this value does not take into account the heat loss from the specimen due to the convective and the radiative heat transfer. Therefore, for the present analysis, an arc efficiency of 80% was assumed. For CO_2 laser beam welding, an absorptivity value of 15% has been reported in the literature (Refs. 7, 21). The absorptivity of the metal surface is a material property that depends on a number of variables such as the nature of the surface, the temperature and the wavelength of the incident radiation. Kou and Wang (Ref. 7) determined calorimetrically the absorptivity of Type 6061 aluminum alloy to be 14%. Khan and DebRoy (Ref. 21) have reported a value of 15% for Type 202 stainless steel. Based on these reported values, an absorptivity of 15% was assumed for the present analysis.

Previous work by several investigators (Refs. 4–14) has shown that $\frac{d\gamma}{dT}$ is the critical variable that significantly influences and often controls the fluid flow in the weld pool. Therefore, a realistic treatment of the surface tension gradient effect is crucial to our understanding of the phenomena that control the weld penetration behavior. The theoretical analysis in this study considers the effect of surface active elements on the weld pool fluid flow by calculating $\frac{d\gamma}{dT}$ as a function of temperature and activity. This approach differs significantly from previous modeling efforts that have considered $\frac{d\gamma}{dT}$ as a specified constant that was assumed to be independent of the temperature. A recently developed surface tension model (Ref. 16) was utilized to evaluate the variation of $\frac{d\gamma}{dT}$ as function of temperature for the two heats of Type 304 stainless steel.

Surface Tension Submodel

Experimental surface tension data are seldom available for any material throughout the temperature range of interest. Sundell, *et al.* (Ref. 9), has obtained surface tension data for different heats of stainless steels with various levels of surface active elements. It must be noted, however, that his results extend only over a limited temperature range from approximately 1800 to 2200 K. Since it is difficult to experimentally obtain surface tension data at all temperatures and compositions of interest, in the calculations presented here a recently developed formalism (Ref. 16) to calculate surface tension was used. The relation between surface tension of the solution and the temperature is given by:

$$\gamma(T) = \gamma_m - A(T - T_m) - R\Gamma_s T \ln[1 + Ka_i] \quad (1)$$

$$K = k_1 \exp\left(\frac{-\Delta H^\circ}{RT}\right), \quad (2)$$

where γ is the surface tension of the solution at the temperature T, γ_m is the surface tension of the pure metal at the melting point T_m, R is the gas constant, Γ_s is the surface excess at saturation, K is the adsorption coefficient, k_1 is a constant which is related to the entropy of segregation, ΔH° is the standard heat of adsorption, and a_i is the activity of the species i in solution.

Temperature coefficient of surface tension $\left(\frac{d\gamma}{dT}\right)$ for an alloy containing a surface active element can be obtained by differentiating Equation 1 with respect to T:

$$\frac{d\gamma}{dT} = -A - R\Gamma_s \ln(1 + Ka_i) - \frac{Ka_i}{(1 + Ka_i)} \frac{\Gamma_s \Delta H^\circ}{T}, \quad (3)$$

where, A is the negative of $\frac{d\gamma}{dT}$ for pure metals.

The temperature coefficient of surface tension was calculated as a function of temperature and activity (wt-% of surface active element) for the entire temperature range of interest. The calculated $\frac{d\gamma}{dT}$ for the two heats of Type 304 stainless steel (90 and 240 ppm sulfur) as a function of temperature is given in Fig. 1. Sulfur present in the base metal segregates preferentially to the weld pool surface, reducing the surface tension of the base metal. For the heat containing 90 ppm of sulfur, $\frac{d\gamma}{dT}$ is positive until about 2200 K. As the melt temperature increases beyond this temperature, $\frac{d\gamma}{dT}$ becomes negative. For a tool steel containing 100 ppm sulfur, Heiple, *et al.* (Ref. 1), has indicated that this critical temperature is 2300 K, as determined by Gogiberidze, *et al.* (Ref. 22). These results are also consistent with the experimental measurements of surface tension for stainless steel by Sundell, *et al.* (Ref. 9). His results show that heats containing surface active elements initially exhibit a positive $\frac{d\gamma}{dT}$. As the temperature of the melt increases beyond a critical temperature, $\frac{d\gamma}{dT}$ becomes negative. Increasing the sulfur content changes the temperature dependence of the surface tension gradient. For example, for a sulfur content of 240 ppm, $\frac{d\gamma}{dT}$ is positive until approximately 2450 K – Fig. 1. As the melt surface temperature increases beyond this temperature, $\frac{d\gamma}{dT}$ becomes negative.

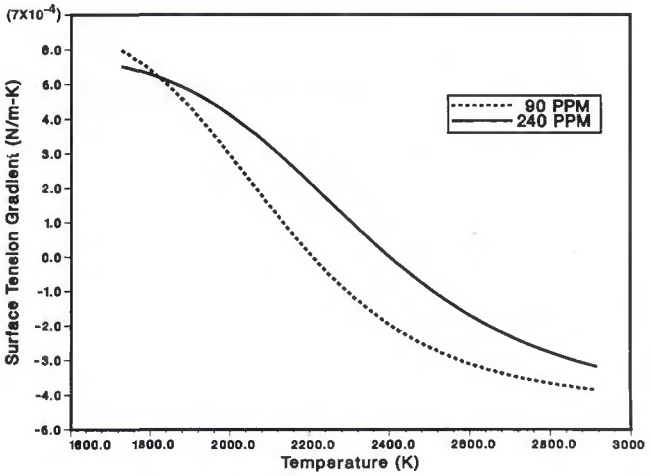

Fig. 1 – Calculated temperature coefficient of surface tension $\frac{d\gamma}{dT}$ as a function of temperature and sulfur content.

Formulation

Figure 2 is a schematic drawing of the weld pool showing the region of interest and the coordinate system chosen for the analysis. The r-component and the z-component of the flow velocities are represented by u and v, respectively. The energy exchange between the heat source and the metal surface produces a molten pool that grows due to conduction and convection. For laser beam welding, the development of the weld pool is governed by buoyancy and surface tension forces. In addition, during GTA welding, the electromagnetic force produced can significantly influence the development of the weld pool. A computational model (Ref. 23) using a finite difference analysis (FDA) was appropriately modified to investigate transient, two-dimensional heat flow and fluid flow problems associated with laser beam and GTA welding processes. The mathematical formulation can consider, depending on the process, buoyancy, electromagnetic and surface tension driving forces in the solution of the overall heat transfer conditions associated with welding. The temperature-dependent surface tension force is calculated based on the sulfur content in the base metal according to the model described in the previous section.

Assumptions in the Model

In formulating the model, the following assumptions were made:

1) The fluid flow and heat transfer in the transverse cross-section inside the molten pool are adequately described by a two-dimensional, time-dependent representation.

2) The power distribution of the heat source is Gaussian.

3) Melting begins when the fusion temperature is reached and is completed when the latent heat of fusion is absorbed.

The Governing Equations

The definitions of all the symbols are presented in the appendix.

Mass Continuity

$$\frac{\partial u}{\partial r} + \frac{\partial v}{\partial z} + \frac{u}{r} = 0 \qquad (4)$$

Momentum

r-direction (radial)

$$\frac{\partial u}{\partial t} + \frac{\partial u^2}{\partial r} + \frac{\partial uv}{\partial z} + \frac{u^2}{r} = -\frac{1}{\rho}\frac{\partial p}{\partial r} + \frac{1}{\rho}F_r + \nu\left[\frac{\partial^2 u}{\partial r^2} + \frac{\partial^2 u}{\partial z^2} + \left(\frac{1}{r}\frac{\partial u}{\partial r} - \frac{u}{r^2}\right)\right] \qquad (5a)$$

z-direction (axial)

$$\frac{\partial v}{\partial t} + \frac{\partial uv}{\partial r} + \frac{\partial v^2}{\partial z} + \frac{uv}{r} = -\frac{1}{\rho}\frac{\partial p}{\partial z} + \frac{1}{\rho}F_z + \nu\left[\frac{\partial^2 v}{\partial r^2} + \frac{\partial^2 v}{\partial z^2} + \frac{1}{r}\cdot\frac{\partial v}{\partial r}\right] \qquad (5b)$$

For laser beam welding, the body force due to the densimetric gradients produced in the weld pool can be expressed as

$$\vec{F} = -\rho\vec{g}\,\beta(\Delta T) \qquad (6a)$$

where, $\vec{g}$ is the acceleration due to gravity, β is the coefficient of thermal expansion and ΔT the change in temperature.

For GTA welding, in addition to the buoyancy force, the electric currents and the induced magnetic fields influence fluid motion and temperature by way of the electromagnetic force. Therefore, for GTA welding, the body force can be expressed as,

$$\vec{F} = -\rho\vec{g}\,\beta(\Delta T) + \vec{J} \times \vec{B} \qquad (6b)$$

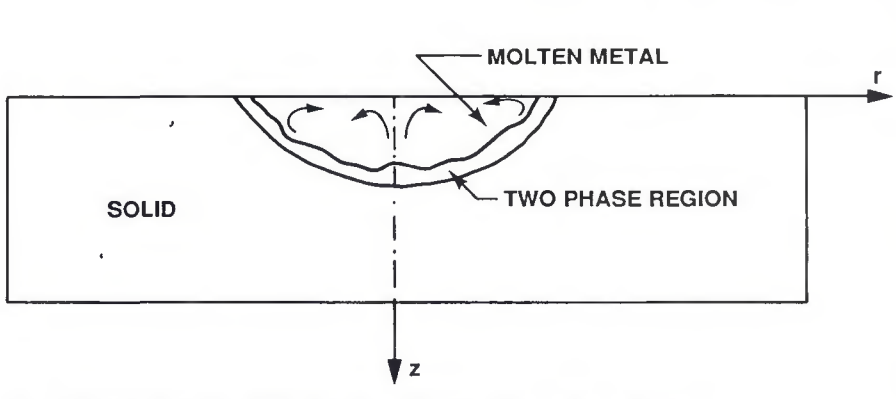

Fig. 2 – Schematic drawing of the weld pool indicating the region of interest.

Table 1—Data Used for Heat Transfer Calculations

Laser power	500 W
Laser beam radius	0.17 mm
Absorptivity	15%
GTA welding current	150 A
GTA welding voltage	14 V
Arc efficiency	80%
Arc radius	3 mm
Liquidus temperature	1725 K
Heat of fusion	0.634×10^2 cal/gm
Boiling temperature	3100 K
Density (liquid)	$7.551 - 1.117 \times 10^{-4}T - 1.506 \times 10^{-7}T^2$ gm/cm^3
A (temperature coefficient of surface tension)	−0.43 gm/s^2 K
Heat of adsorption	-1.88×10^5 kJ/kg mole
k_1	0.00318
surface excess at saturation	1.33×10^{-8} kg mole/m^2
Effective viscosity of molten metal	0.5 gm/cm s
Effective thermal conductivity of molten metal	0.37 cal/cm-s-K
Heat transfer coefficient at the solid surface	3.15×10^{-4} $\Delta T^{0.25}$ cal/s cm^2 K

where, $\vec{J}$ is the current density vector and $\vec{B}$ is the magnetic flux vector.

Energy

The enthalpy, rather than the temperature, was considered as the dependent variable in the energy equation. Here, the latent heat is included in the definition of enthalpy. The energy equation in two-dimensions may be expressed as

$$\frac{\partial H}{\partial t} + u\frac{\partial H}{\partial r} + v\frac{\partial H}{\partial z} = \frac{k}{\rho C_p}\left[\frac{\partial^2 H}{\partial r^2} + \frac{\partial^2 H}{\partial z^2}\right] + S_H(r) \quad (7)$$

The above equation is used to calculate the temperature distribution in the workpiece, with the help of a relationship for enthalpy as a function of temperature covering both the solid and liquid phases.

The source term in the above equation, $S_H(r)$, represents the absorption of energy from the heat source, given by,

$$S_H(r) = \frac{\eta \cdot q(r)}{\rho \gamma_d} \quad (8)$$

The fraction of incident energy absorbed is represented by an efficiency factor, η.

The heat flux, q(r), was assumed to be Gaussian in nature and is given by the following equation,

$$q(r) = \frac{3Q}{\pi r_b^2} e^{-[3r^2/r_b^2]} \quad (9)$$

Boundary Conditions

Thermal Boundary Conditions

1) The heat transfer between the surface of the sample and the surroundings is a specified input parameter and is given by Equation 8.

2) In the radial plane of the sample, since symmetry was assumed about the heat source, there is no heat flow across the plane of symmetry.

3) The heat transfer at the bottom and the sides of the sample is calculated by equating the conduction heat flux with the heat flux due to convection from the sample surface.

Dynamic Boundary Conditions

1) In the transverse cross-section of the pool, the mass transfer across the centerplane is zero (u = 0) since symmetry is assumed.

2) At the surface of the pool, the Marangoni effect was incorporated by equating the shear stress at the surface to the gradient of surface tension.

3) All velocities at the solid/liquid interface are zero since no-slip conditions are assumed.

An outline of the solution procedure, information on the grids, a discussion of stability, convergence and the accuracy of the solution for computations are presented in the appendix. Data used for computations are in Table 1.

Results and Discussion

The detailed information on the fluid flow and the accompanying heat transfer that occur during stationary GTA and laser beam welding of a 30 × 30 × 6-mm Type 304 stainless steel specimen was obtained by numerically solving the mathematical models that represent the essential physical features of the processes. Two heats of Type 304 containing 90 and 240 ppm of sulfur were considered in this investigation. The different levels of sulfur content can significantly alter the fluid flow and heat transfer in the weld pool, thereby altering the weld pool shape and size. Therefore, the computational model was used to simulate the welding processes for both heats in order to quantitatively understand the effect of different sulfur contents on the fluid flow, the heat transfer and the weld geometry.

GTAW Process

The flow and temperature fields during GTA welding were simulated for both heats (90 and 240 ppm sulfur) of Type 304 stainless steel. First, the computed results for the heat containing 90 ppm sulfur are presented. The results of the fluid flow calculations in the weld pool due to the simultaneous interaction of buoyancy, electromagnetic and surface tension gradient effects are presented in Figs. 3 and 4 for stationary spot welds. Figure 3 shows the calculated flow field in the weld pool after 2 s. The major vortex near the weld pool surface is dominated by the surface tension gradient effect causing a radially outward flow. Away from the weld pool surface, near the centerline of the weld pool, the flow field is controlled by the electromagnetic force. The maximum radial surface velocities are of the order of 0.12 m/s. The calculated velocities appear to agree qualitatively with earlier theoretical investigations. Previous theoretical investigations on the fluid flow in weld pools during GTA welding of a wide variety of materials have reported surface velocities

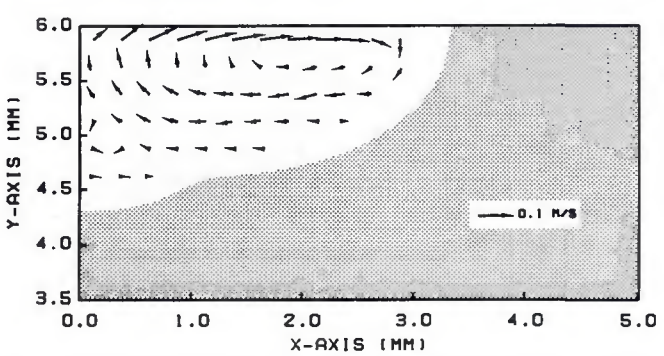

Fig. 3—Calculated flow field, after 2 s, during GTA welding of Type 304 stainless steel containing 90 ppm sulfur.

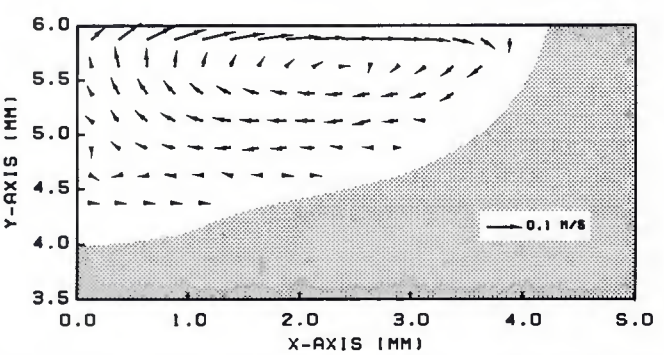

Fig. 4—Calculated flow field, after 5 s, during GTA welding of Type 304 stainless steel containing 90 ppm sulfur.

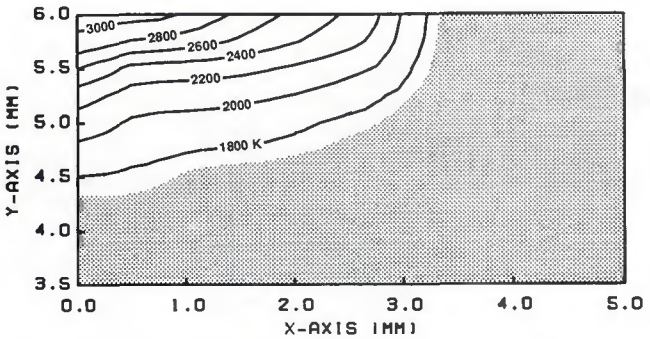

Fig. 5 — Calculated temperature field, after 2 s, during GTA welding of Type 304 stainless steel containing 90 ppm sulfur.

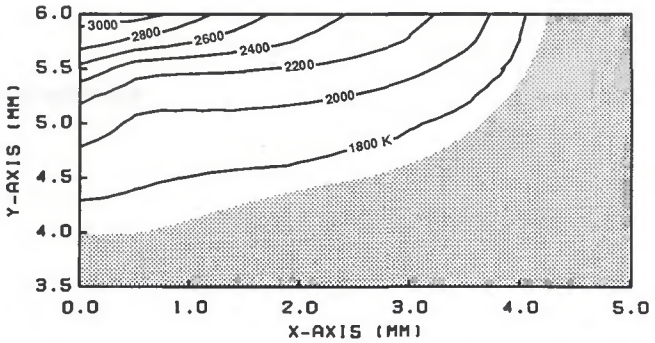

Fig. 6 — Calculated temperature field, after 5 s, during GTA welding of Type 304 stainless steel containing 90 ppm sulfur.

ranging from 0.05 m/s (Ref. 24) to 1 m/s (Refs. 8, 10, 11, 23). All these studies assumed a constant $\frac{d\gamma}{dT}$ ranging from -0.01×10^{-3} N/m · K to -0.35×10^{-3} N/m · K. Particularly, the higher velocities of 1 m/s were obtained for a $\frac{d\gamma}{dT}$ of -0.35×10^{-3} N/m · K (Refs. 8, 10, 11). The calculated flow field after 5 s shows no apparent change in behavior of the weld pool development (Fig. 4) relative to the results after 2 s. However, the weld pool expands by about 25%. The flow field is once again radially outward at the weld pool surface, resulting in shallow penetration. The maximum surface velocities remain unchanged.

The calculated temperature fields after 2 and 5 s are presented in Figs. 5 and 6, respectively. The simulated results clearly show the influence of convection on the temperature distribution in the weld pool. Even though there exist opposing surface tension gradient effects on the weld pool surface, the negative $\frac{d\gamma}{dT}$ that is present over much of the weld pool surface, associated with the higher temperatures, prevails and controls the surface flows. The calculated flow field is radially outward, transporting heat from the center to the periphery. Deeper within the weld pool, the effect of the surface flows on the temperature fields diminishes. This is particularly evident at the center of the pool where the inward flow due to the electromagnetic force transports relatively hot liquid from the periphery to the interior, causing the isotherms to be deeper at these locations. Outside the weld pool, the transport of heat is controlled by conduction.

The results of the previous experimental investigations (Refs. 1, 15) studying the effect of sulfur on the weld pool fluid flow suggest that the amount of sulfur has to exceed a critical level before observing flow reversal. Heiple, *et al.* (Ref. 1), has reported that the addition of 50 ppm of sulfur increased the depth/width ratio of a GTA weld in 21-6-9 stainless steel by over 80%, suggesting an inward flow of the liquid melt in the weld pool. Considering that the alloy used in the present investigation has 90 ppm sulfur, it is surprising that the calculated results indicate an outward flow instead of a radially inward flow as suggested by the earlier investigations. This discrepancy is likely due to the fact that previous experimental results were obtained for linear (moving arc) welds. The GTA welding parameters in these earlier studies were a welding current of 150 A and a travel speed of 2.12 mm/s (5 in./min) (Ref. 1). For the same welding current (150 A), the surface temperatures in the weld pool would be significantly lower for a moving arc weld (due to lower heat input). For example, Sundell, *et al.* (Ref. 9), has reported peak temperatures of $\approx$ 2100 K for linear welds on stainless steels. Under such conditions, the flow field would be radially inward since $\frac{d\gamma}{dT}$ would be positive everywhere on the melt surface — Fig. 1. On the other hand, the calculated results from this study show that much of the weld pool surface is above 2200 K, and therefore, a negative $\frac{d\gamma}{dT}$, which causes a radially outward flow, is present.

In the interior of the weld pool, the electromagnetic force prevails, resulting in a minimal flow in the radially inward direction — Figs. 3 and 4. The inflection in the fusion zone interface is due to this flow reversal, causing increased local penetration. The calculated velocities in the interior of the weld are at least an order of magnitude less than the surface velocities. For the conditions investigated, the overall effect of the electromagnetic force on the weld pool development is relatively weak compared to the effect of the surface tension gradient. This is to be expected since the welding current used in this investigation is relatively low. Heiple, *et al.* (Refs. 13–15), has shown that for low welding currents (<150 A) the surface tension gradient at the weld pool surface is the dominant force driving fluid flow in the weld pool. Increasing the welding current above 150 A may increase the depth/width ratio by increasing the momentum and thermal transport due to electromagnetic force. In addition, the increased heat input due to any increase in welding current would cause the weld pool to be wider, thereby reducing the temperature gradient. This would in turn reduce the surface tension force opposing the electromagnetic force. The increase in welding current is not expected to have any significant effect on $\frac{d\gamma}{dT}$ as the peak temperature in the pool is already at the boiling point of the metal. At these high temperatures, $\frac{d\gamma}{dT}$ is not very sensitive to temperature changes.

The calculated values of the weld penetration depth and width until full penetration, for GTA welds, are plotted as a function of time in Fig. 7. Initially, the results show shallow weld penetration with a relatively low depth/width ratio. The results show that the width of the pool increases rapidly to about 70% of its width at full penetration in 10% of the time it takes to achieve full penetration. With further increase in weld duration, the width increases slowly with time. Initially, the radially outward flow transports heat from the center to the periphery of the weld at a much faster rate than the base metal can conduct heat away from the interface. This results in the rapid lateral development of the weld pool. As the width of the weld pool increases, the area of the lateral interface between solid and the liquid increases, allowing more efficient heat removal from lateral faces of the weld pool. This results in slower growth along this direction with continued heating.

The penetration depth, on the other hand, increases more steadily with increasing weld duration until about 9 s. Beyond this time, the penetration depth increases rapidly until full penetration is achieved at 12 s. The location where the slope of the depth curve changes rapidly represents a change in the mechanism that controls the development of the weld pool. For example, the development of the weld pool is initially controlled by convective heat transfer in the weld pool. This is evidenced by shallow weld pene-

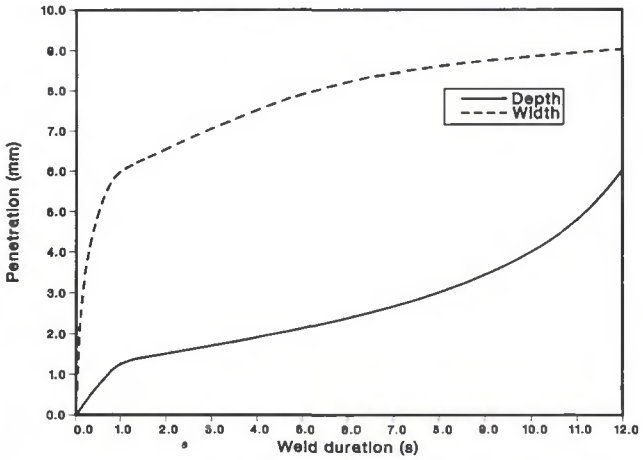

Fig. 7 — Calculated penetration depth and width during GTA welding of Type 304 stainless steel containing 90 ppm sulfur.

tration (Figs. 3 and 4) and the low depth/width ratios — Fig. 7. However, after sufficient time has elapsed, the weld pool development (weld penetration) is controlled by conductive heat transfer in the base metal. The finite size of the specimen (the thickness of the material is only 6 mm), leads to inefficient heat transfer (lower thermal gradient) in the base metal directly below the weld pool. This causes the material below the pool to heat up rapidly, resulting in deeper penetration, as seen in Fig. 7. At the same time, toward the sides of the weld pool, at the fusion zone interface, the amount of energy transferred from the weld pool to the base metal is quickly transported to the bulk of the specimen by conduction heat transfer. Therefore, with continued heating, the width of the weld pool increases relatively slowly.

Variable depth of penetration during the welding of different heats of the same material (compositions within the specified allowable range) is a significant problem that has received much attention in recent times. The depth of penetration achieved during welding can significantly influence the quality and the reliability of the weldment. Often, the critical variable that controls the variation in the weld pool size and shape is the amount of minor elements that are present in commercially available material. In iron-base alloys, sulfur and oxygen are the most important surface active elements commonly found. With improved steel-making practice, the amount of minor elements such as sulfur in steel has been greatly reduced. Unfortunately, the typical levels of sulfur content in these alloys fall in the region where small variations can cause $\frac{d\gamma}{dT}$ to change from negative to positive during welding. Consequently, these small variations in the sulfur level can cause considerable variation in the weld penetration. The simulated results of the fluid flow and the heat transfer during GTA welding of the heat containing 240 ppm sulfur are presented next to illustrate the effect of changes in sulfur content.

In order to quantitatively evaluate the effect of the higher sulfur content on the weld penetration and geometry, the flow and temperature fields after 2 and 5 s were computationally modeled for a sulfur content of 240 ppm. The $\frac{d\gamma}{dT}$ was evaluated for the higher sulfur content as a function of the temperature — Fig. 1. Figure 8 shows the calculated flow field after 2 s. The results indicate the significant effect of sulfur on the fluid flow pattern. Instead of the simple inward flow as suggested by earlier investigations, the results indicate a complex bifurcated flow pattern with radially inward and outward loops on the surface of the weld pool. Such complex flow patterns are to be expected since $\frac{d\gamma}{dT}$ changes its sign at 2450 K — Fig. 1. The radially inward flow due to the positive $\frac{d\gamma}{dT}$ at the cooler periphery of the weld pool opposes the flow due to the negative $\frac{d\gamma}{dT}$ that prevails over much of the weld pool surface. Therefore, in the presence of the higher sulfur content, the heat from the arc is not transported to the periphery as efficiently as in the previous case, resulting in a reduction in width of pool.

Figure 9 shows the calculated flow field after 5 s. With continued heating beyond 2 s, the positive $\frac{d\gamma}{dT}$ at the periphery significantly influences the local flow field. As a result, the radially inward flow near the solid-liquid interface increases with time. The predicted flow field significantly influences the development of the weld pool as can be seen from Fig. 9. The radially outward loop near the centerline transports heat radially outward from the center of the pool. However, in this case, the relatively hot liquid metal is met by a radially inward flow that is transporting heat from the sides to the interior. The ensuing convective heat transfer produces an almost cylindrical weld pool with increased depth of penetration primarily at the periphery instead of at the center of the weld pool.

The calculated temperature fields after 2 and 5 s (for the heat containing 240 ppm sulfur) are presented in Figs. 10 and 11, respectively. After 2 s, the calculated temperature distribution is similar to that obtained for the lower sulfur content. The

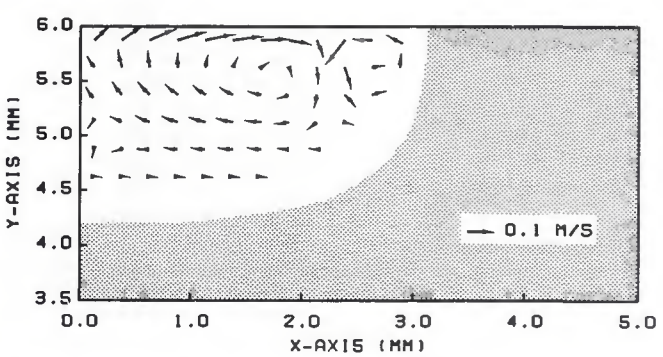

Fig. 8 — Calculated flow field, after 2 s, during GTA welding of Type 304 stainless steel containing 240 ppm sulfur.

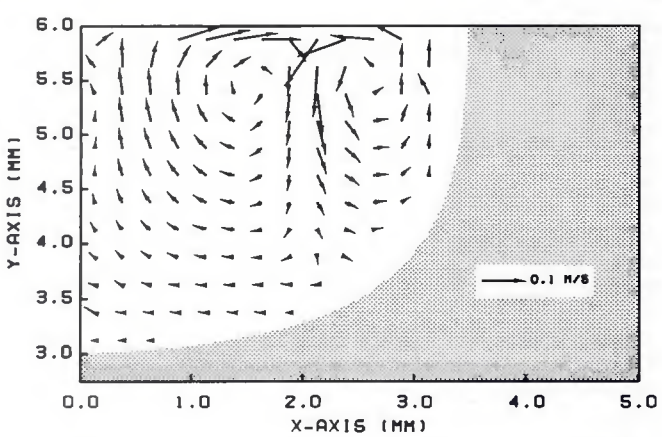

Fig. 9 — Calculated flow field, after 5 s, during GTA welding of Type 304 stainless steel containing 240 ppm sulfur.

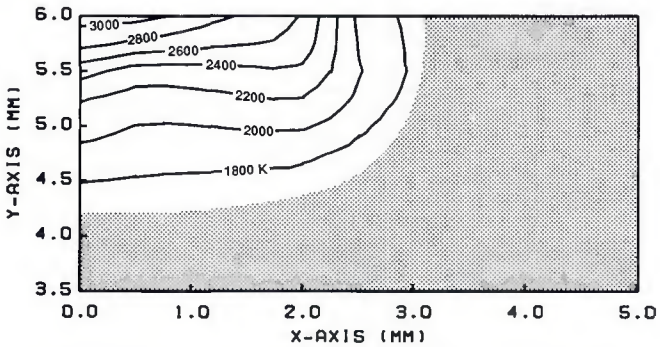

Fig. 10 — Calculated temperature field, after 2 s, during GTA welding of Type 304 stainless steel containing 240 ppm sulfur.

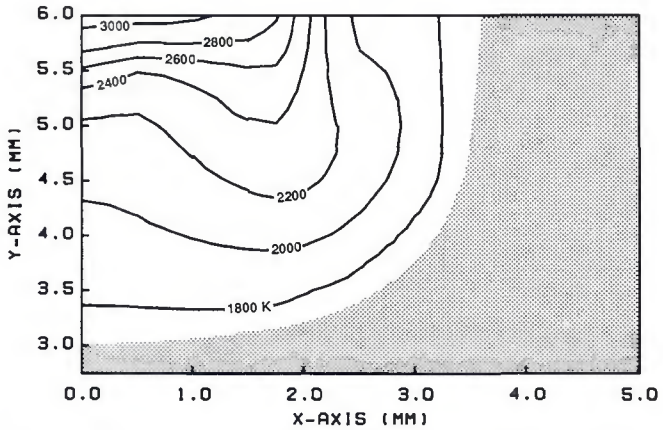

Fig. 11 — Calculated temperature field, after 5 s, during GTA welding of Type 304 stainless steel containing 240 ppm sulfur.

negative $\frac{d\gamma}{dT}$ over much of the weld pool surface causes an outward flow, transporting heat from the welding arc to the periphery of the weld pool. This results in relatively shallow isotherms in the weld pool. At the same time, the radially inward flow at the periphery, locally, opposes this flow. This flow loop is considerably smaller than the outward flow loop and does not have any significant effect on the temperature field after 2 s. However, after 5 s, the results show the significant influence the modified flow (due to the higher sulfur content) has on the temperature distribution in the weld pool. The resulting temperature field is considerably different and has a profound influence on the bead shape.

The results presented in this section clearly show the influence of a surface active element such as sulfur on the flow and temperature field during stationary welding, which affect the ultimate weld pool shape and size. There is overwhelming experimental evidence that small variations in sulfur can cause significantly different penetration behavior. The present investigation confirms that sulfur can cause variations in the bead geometry by altering the surface tension gradient, and thereby altering the fluid flow and convective heat transfer in the weld pool. However, the effect of sulfur on the flow reversal and the bead geometry is not as pronounced in this study as that reported by the earlier investigations (Refs. 1, 12-15). This relatively weak influence of sulfur on the bead geometry is attributed to the higher surface temperatures observed during stationary welding compared to linear welding. To illustrate this effect, the flow field and the temperature field during linear GTA welding were calculated in a two-dimensional plane along the welding direction, for the heat containing 240 ppm sulfur. The welding parameters used were: welding current of 150 A, arc voltage of 14 V, and a welding speed of 2.5 mm/s. The results of the calculation are presented in Fig. 12. Figure 12A shows a radially inward flow in the weld pool, as suggested by previous experimental investigations, resulting in increased depth of penetration. Figure 12B shows the calculated temperature distribution in the weld pool. The calculated peak temperature at the surface is on the order of 2500 K, which implies that a positive $\frac{d\gamma}{dT}$ exists over most of the weld pool surface. This explains the calculated inward flow in the case of linear GTA welding.

The results presented in the previous sections clearly show that while sulfur in the base metal can alter the flow field, and thereby influence the weld penetration, the extent of this effect is a strong function of the temperature field in the weld pool. In order to illustrate the importance of considering $\frac{d\gamma}{dT}$ as a function of temperature and sulfur content, the fluid flow and the consequent weld pool shape and size were calculated assuming a constant positive $\frac{d\gamma}{dT}$ of 0.15×10^{-3} N/m · K. The computed flow field and temperature field for GTA welding after 2 s are presented in Fig. 13. The results show an inward flow pattern causing very large depth of penetration.

A method currently employed by some fabricators to minimize variations in penetration is to increase the sulfur content of the alloys. However, sulfurization can have a deleterious effect on the cracking tendency of the weld and properties of the welded joint. Therefore, this may not be a viable method for controlling variable penetration in welded joints for certain critical applications. Sundell, *et al.* (Ref. 9), investigated the effect of increasing the sulfur content on hot-crack sensitivity of stainless steels. His results showed that sulfur added to the weld bead could increase the possibility of hot-cracking in welds that solidify in the primary austenite mode. A possible alternative method for controlling variable penetration could be through process control. For critical applications, where sulfurization can cause detrimental metallurgical effects, it may be possible to consistently produce a negative $\frac{d\gamma}{dT}$, and thus, consistent depth of penetration by increasing the surface temperature of the weld pool.

In general, the results indicate that the weld pool development and growth in

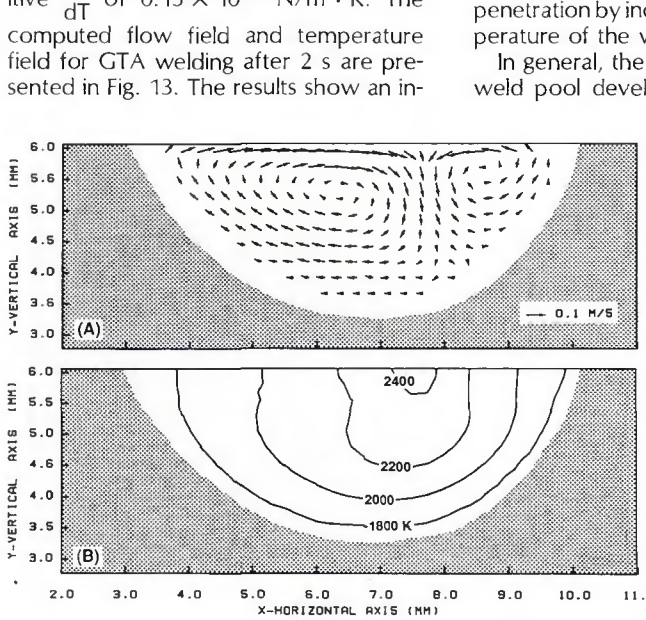

Fig. 12 — Calculated heat flow and fluid flow during linear GTA welding of Type 304 stainless steel containing 240 ppm sulfur (150 A, 14 V, 2.5 mm/s). A — Flow field; B — temperature field.

GTA welding is controlled by convective heat transfer, which is dominated by surface tension gradient driven flows. The surface tension gradient driven flow can be modified locally, at interior locations, by the electromagnetic force, resulting in enhanced penetration below the arc. In addition, the finite size of the specimen and its geometry may influence the heat transfer in the specimen and can, in some instances, control the development of the weld pool.

Laser Beam Process

The flow and temperature fields during laser beam welding were simulated for both heats of Type 304 stainless steel. First, the computed results for the heat containing 90 ppm sulfur are presented. Figure 14 shows the calculated flow field in the weld pool after 2 s. The results show a single coherent vortex during laser beam welding. As discussed earlier, during laser beam welding, the driving forces for convection in the weld pool are surface tension and buoyancy. Due to the high surface temperature, $\frac{d\gamma}{dT}$ is largely negative, causing a radially outward flow at the weld pool surface. This flow is augmented by the buoyancy driven flows in the interior of the pool. In the absence of any significant opposing forces, the resulting fluid flow pattern consists of a single coherent loop. The maximum radial velocity at the weld pool surface is of the order of 0.7 m/s. The higher velocity is to be expected as the temperature gradient on the weld pool surface is significantly higher than during conventional GTA welding. The radially outward flow produces a relatively shallow weld pool (depth/width ratio of 0.28) by transferring the heat from the center to the periphery. Interestingly, the depth/width ratio of 0.28 for laser beam welds is close to the ratio of 0.27 obtained for GTA welds after 5 s. Figure 15 shows the calculated temperature field in the weld pool after 2 s of welding. The calculated temperature distribution is similar to that obtained for GTA welding. The negative $\frac{d\gamma}{dT}$ over much of the weld pool surface prevails and controls the surface flows, transporting heat from the center to the periphery. Consequently, the calculated isotherms are shallow and wide.

The predicted results obtained after 5 s of welding are very similar to those obtained after 2 s and, therefore, are not presented here. During laser beam welding, the use of a laser beam focused on a very small area results in higher power density causing a rapid increase in the local temperature of the material. At the same time, the energy supplied to the weld is relatively low, producing a small weld in comparison to the overall size of the specimen. Therefore, a quasi-steady state is achieved very quickly as the energy supplied to the weld is rapidly conducted away by the base metal.

Figure 16 shows the calculated flow field after 2 s for the heat containing 240 ppm sulfur. The predicted flow field is radially outward, even in the presence of the higher sulfur content, resulting in a relatively shallow pool. The positive $\frac{d\gamma}{dT}$ near the cooler periphery of the weld pool produces a radially inward flow. However, this inward flow is relatively weak and does not significantly influence the overall heat transfer or the fluid flow in the weld pool. This is to be expected as the surface temperature in the weld pool would be considerably higher during welding with a high energy laser beam. Even though the flow field consists of two convective vortices, the results show very little difference in the overall shape or size of the pool compared to the lower sulfur content weld. Therefore, minor variations in surface active elements (within the allowable limits) are not expected to produce any major variations in the penetration depth. The maximum surface velocities are of the order of 0.7 m/s. Figure 17 shows the temperature distribution in the weld pool. The inward flow at the periphery of the pool slightly influences the temperature distribution. The predicted results obtained after 5 s of welding are very similar to those obtained after 2 s, and therefore, are not presented here.

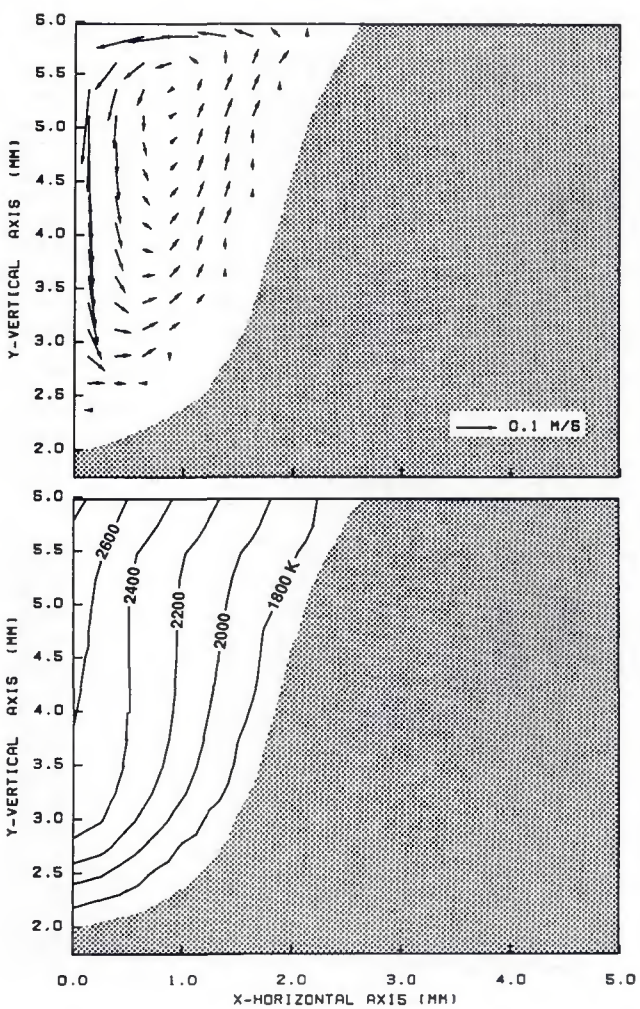

Fig. 13—Calculated heat flow and fluid flow, after 2 s, during stationary GTA welding of Type 304 stainless steel assuming a constant $\frac{d\gamma}{dT}$ of 0.15×10^{-3}. A—Flow field; B—temperature field.

Calculated Cooling Rates

The rate at which a material cools after welding significantly influences the final solidification structure and the mechanical properties of the weld. Variations of the cooling rate cause modifications of the solidification rate, thereby influencing the solidification front morphology. The average cooling rate at any location in a weld is a function of the material properties, the welding process and the heat input. The exact measurement of cooling rates in a weld pool during and after welding is difficult; therefore, the available data in the literature are scarce. Recent computational modeling efforts have provided a reasonable alternative to direct measurements by allowing the prediction of the cooling rates at any location in the weld pool. Several investigators have numerically calculated or indirectly estimated the cooling rates for various welding situa-

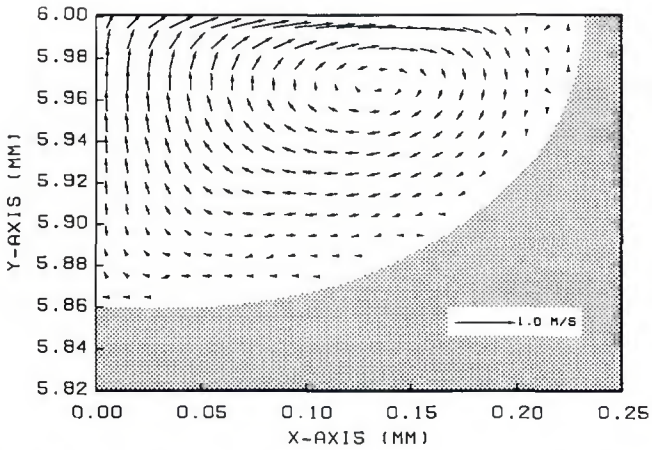

Fig. 14 — Calculated flow field, after 2 s, during laser beam welding of Type 304 stainless steel containing 90 ppm sulfur.

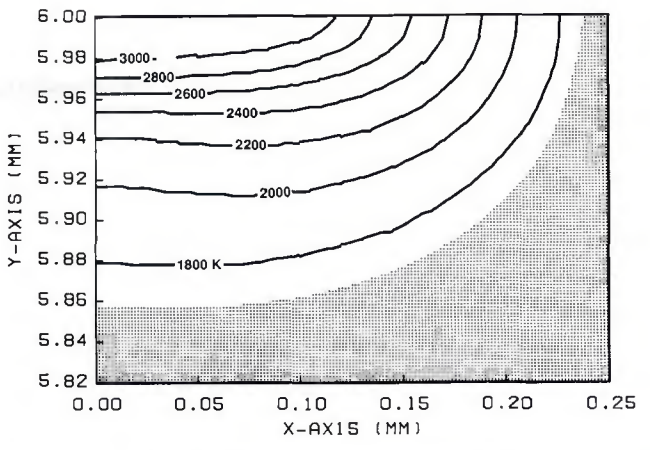

Fig. 15 — Calculated temperature field, after 2 s, during laser beam welding of Type 304 stainless steel containing 90 ppm sulfur.

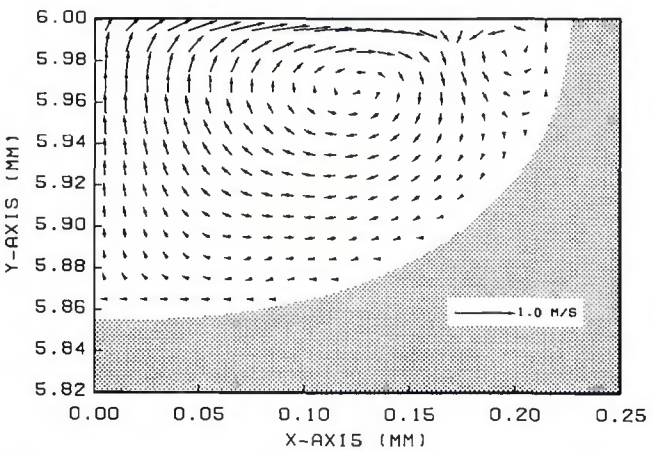

Fig. 16 — Calculated flow field, after 2 s, during laser beam welding of Type 304 stainless steel containing 240 ppm sulfur.

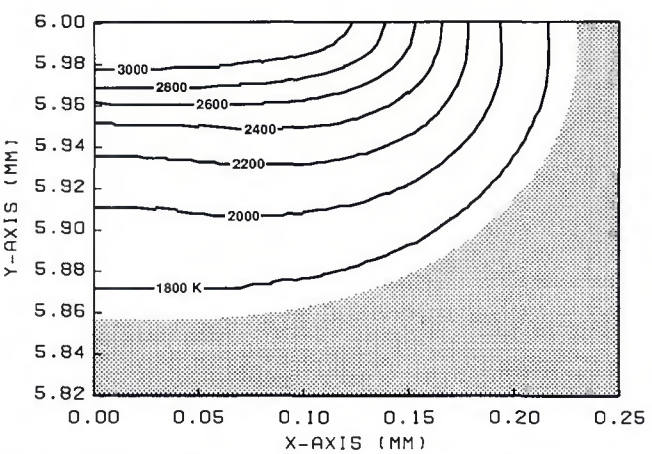

Fig. 17 — Calculated temperature field, after 2 s, during laser beam welding of Type 304 stainless steel containing 240 ppm sulfur.

tions. Katayama, *et al.* (Ref. 25), reported cooling rates of $\approx 1000\,K \cdot s^{-1}$ during the solidification of conventional GTA welds. The present authors have modeled the heat transfer that occurs during pulsed laser beam welding of several stainless steels (Refs. 26, 27). For the range of welding speeds and heat input considered in these previous investigations, the predicted cooling rates ranged from 0.56 to $8.8 \times 10^5 K \cdot s^{-1}$. Therefore, the available information in the literature suggests that the cooling rates vary widely, as would be expected, depending on the processing conditions and the material.

Typically, we are concerned with the cooling rates at the solidification temperature. The cooling rates were calculated as the solid/liquid interface passed through particular locations in the weld pool. The calculations indicate, as expected, that the cooling rates experienced were highest along the periphery of the weld pool and lowest at the center. For conventional GTA welding, after 5 s, the calculated cooling rate near the surface of the weld pool at the solid-liquid interface was 1400 $K \cdot s^{-1}$. At the same time, the cooling rate experienced by the weld metal during the final solidification near the center of the weld pool was 850 $K \cdot s^{-1}$. In general, the cooling rates experienced by the weldment decreased with increasing weld duration. This is to be expected, since the finite size of the specimen would cause the overall temperature of the base metal to increase with increasing weld duration.

The cooling rates experienced by the laser beam welds were significantly higher. The liquid metal at the weld periphery experiences cooling rates of $\approx 1.0 \times 10^5$ $K \cdot s^{-1}$, as it solidifies. The calculated cooling rates experienced by the weld metal, as it solidified, ranged from 0.26 to 1.0×10^5 $K \cdot s^{-1}$. There were no significant variations in the cooling rates during weld solidification after 2 and 5 s of welding, since a quasi-steady state is achieved by 2 s. Comparing the cooling rates to the previously reported values, the present calculations are within the same order of magnitude.

Summary and Conclusions

A theoretical evaluation of the development of the weld pool during conventional GTA and laser beam welding of Type 304 stainless steel was carried out. In the present investigation, the effect of sulfur on the fluid flow and heat transfer was considered by calculating $\frac{d\gamma}{dT}$ as a function of temperature and sulfur concentration. Sulfur in the base metal causes $\frac{d\gamma}{dT}$ to be positive at relatively low temperatures. As the surface temperature increases beyond a particular temperature, even with sulfur, $\frac{d\gamma}{dT}$ changes from a positive value to a negative value.

The results confirm the significant influence of convective heat transfer on the development of the weld pool. It has been shown that surface tension gradient driven flow dominates the fluid flow and controls the development of the weld pool for both welding processes. During conventional GTA welding, the strong electromagnetic force can influence the flow locally, at interior locations, enhancing the penetration directly below the arc. During GTA welding, the maximum velocities observed on the weld pool surface were of the order of 0.12 m/s. On the other hand, the higher temperature gradi-

ents that exist on the weld pool surface during laser beam welding produced higher surface velocities of the order of 0.7 m/s.

For both welding processes, the results of the computer simulation show relatively shallow welds (low depth/width ratios) for the heat with the lower sulfur content. After 5 s, the depth/width ratio for the laser beam welds was ≈ 0.28 and for GTA welds was ≈ 0.27. Increasing the sulfur content of the Type 304 alloy increased the weld penetration during GTA welding. The observed increase in penetration was considerably less than the values reported by earlier investigations. During laser beam welding, the increased sulfur content did not have any appreciable effect on the weld pool size or shape.

During stationary welding, the calculated flow field and the consequent development of the pool varied significantly from the expected results based on earlier experimental investigations. The calculated flow field was radially outward even when the material contained significant levels of sulfur. It has been shown that the weld penetration and the aspect ratio are not determined solely on the basis of the amount of surface active element in the base metal, but rather due to a combination of the surface active element concentration and the temperature distribution. The absence of any major effect of sulfur on the laser weld pool shape and size can be attributed to the considerably higher temperatures that exist on the pool surface of the welds. The model correctly predicted the expected inward flow during linear GTA welding. During linear welding the peak surface temperatures are considerably lower, and consequently, a positive $\frac{d\gamma}{dT}$ exists on the weld pool surface causing the inward flow.

The calculated cooling rates at the solidification temperature for both welding processes were higher at the edge than at the bottom center or the top center of the pool. For the welding conditions investigated experimentally, the calculated cooling rates for GTA welding ranged from a minimum of about 850 $K \cdot s^{-1}$ at the center to about 1400 $K \cdot s^{-1}$ at the periphery of the weld. In general, calculated cooling rates decreased with increased weld duration (increased heat input). At the same time, calculated cooling rates for laser beam welds ranged from 0.26×10^5 $K \cdot s^{-1}$ at the center to 1.0×10^5 $K \cdot s^{-1}$ at the periphery.

Appendix

Definition of Symbols

a_i = activity of the species i
$\underline{A}$ = constant
$\vec{B}$ = magnetic flux vector
c_p = specific heat
$\vec{f_b}$ = body force
$\vec{g}$ = gravitational constant
H = enthalpy
ΔH° = heat of adsorption
$\vec{I}$ = current density vector
K = adsorption coefficient
K_1 = constant
p = pressure
$\vec{q_s}$ = heat transfer flux
Q = laser power
r_b = effective radius of heat flux
R = gas constant
t = time
T_m = melting temperature
$\dot{T}$ = cooling rate
u = radial velocity
v = axial velocity
y_d = absorption depth
β = coefficient of thermal expansion
ϵ = absorptivity
γ = surface tension of the solution
γ_m = surface tension of the pure metal at T_m
Γ_s = Surface excess at saturation
κ = thermal conductivity
υ = kinematic viscosity
ρ = density

Method of Solution

The governing equations and the boundary conditions were expressed in finite difference form and solved on a line-by-line basis utilizing the tri-diagonal matrix algorithm (TDMA). First, the energy equation was solved for the entire computational domain using the TDMA, starting with the known values of enthalpy corresponding to room temperature. The pool geometry was determined based on the calculated values of enthalpies and the momentum equations solved within this molten pool. The continuity equation was identically satisfied to within 1% of a specified reference mass divergence. The calculated enthalpies and velocities were updated for each time level.

The mathematical model used a 50×40 nonuniform, fixed rectangular grid system for the calculation of enthalpies and velocities. Finer grids were utilized near the surface of the specimen where steep velocity gradients are induced by the surface tension gradient. Far away from the surface, a relatively coarse grid was utilized.

Stability, Convergence and Accuracy of the Numerical Scheme

Unconditional stability was obtained since the solution procedure was an implicit one. Thus, an unduly small time increment mandated by an explicit scheme is not required.

The maximum permissible mass imbalance in each cell was 1% of a reference mass divergence. The value of this reference divergence was taken as 5000 s^{-1} for a minimum grid spacing of 0.01 mm and a typical velocity difference of 0.01 m/s. The momentum and enthalpy convergence was achieved when u, v, and H satisfied the momentum, continuity and enthalpy equations simultaneously. The maximum permissible relative difference between the velocities at each location obtained from the solution of the continuity and momentum equations was 0.01.

A parametric study indicated that time increments less than 0.001 s did not give any different results for a minimum grid spacing of 0.01 mm. Hence, for all calculations, the time increment was taken as 0.001 s.

Acknowledgments

The authors would like to thank S. K. Iskander and M. Maguire for reviewing the manuscript. The research was sponsored by the Div. of Materials Sciences, U. S. Dept. of Energy, under contract DE-AC05-84OR21400 with Martin Marietta Energy Systems, Inc.

References

1. Heiple, C. R., and Roper, J. R. 1982. Mechanism for minor element effect on GTA fusion zone geometry. *Welding Journal* 61(4):97-s.

2. Tsai, N. S., and Eagar, T. W. 1984. *Modeling of Casting and Welding Process II*, p. 317.

3. Athey, D. R. 1980. A mathematical model for fluid flow phenomena in weld pools. *Journal of Fluid Mechanics*. Vol. 98, p. 787.

4. Oreper, G. M., and Szekely, J. 1984. Heat and fluid flow phenomena in weld pools. *Journal of Fluid Mechanics*. Vol. 147, p. 53.

5. Chan, C., Mazumder, J., and Chen, M. M. 1984. A two-dimensional transient model for convection in laser melted pools. *Metall. Trans.* Vol. 15A, p. 2175.

6. Kou, S., and Sun, D. K. 1985. Fluid flow and weld penetration in stationary arc welds. *Metall. Trans.* Vol. 16A, p. 203.

7. Kou, S., and Wang, Y. H. 1986. Three-dimensional convection in laser melted pools. *Metall. Trans.* Vol. 17A, p. 2265.

8. Kou, S., and Wang, Y. H. 1986. Weld pool convection and its effect. *Welding Journal* 65(3):63-s.

9. Sundell, R. E., Correa, S. M., Harris, L. P., Solomon, H. D., Wojcik, L. A., Savage, W. F., Walsh, D. W., and Lo, G-D. 1986. Minor element effects on gas tungsten arc weld penetration. GE Report No. 86SRD013.

10. Zacharia, T., Eraslan, A. H., and Aidun, D. K. 1988. Modeling of non-autogenous welding. *Welding Journal* 67(1):18-s.

11. Zacharia, T., Eraslan, A. H., and Aidun, D. K. 1988. Modeling of autogenous welding. *Welding Journal* 67(3):53-s.

12. Heiple, C. R., Roper, J. R., Stagner, R. T., and Alden, J. J. 1983. Surface active element effects on the shape of GTA, laser and electron beam welds. *Welding Journal* 62(3):72-s.

13. Heiple, C. R., and Roper, J. R. 1981. Effect of selenium on GTAW fusion zone geometry. *Welding Journal* 60(8):143-s.

14. Heiple, C. R., and Burgardt, P. 1985. Effects of SO_2 shielding gas additions on GTA weld shape. *Welding Journal* 64(6):159-s.

15. Heiple, C. R., and Roper, J. R. 1981. Effects of minor elements on GTAW fusion zone

shape. *Trends in Welding in the United States,* Ed. S. A. David, ASM International, Materials Park, Ohio. p. 489.

16. Sahoo, P., DebRoy, T., and McNallan, M. J. 1988. Surface tension of binary metal-surface active solute systems under conditions relevent to welding metallurgy. *Metall. Trans.* Vol. 19B, p. 483.

17. Key, J. F., Chan, J. W., Smartt, H. B., and McIlwain, M. 1983. Process variable influence on arc temperature distribution. *Welding Journal* 62(7):179-s.

18. Pavelic, V., Tanbakuchi, R., Uyehara, O. A., and Meyers, P. S. 1969. Experimental and computed temperature histories in gas tungsten-arc welding of thin plates. *Welding Journal* 48(7):295-s.

19. Smartt, H. B., Stewart, J. A., and Einerson, C. J. 1985. Paper presented at the 66th Annual AWS Convention, Las Vegas, Nev.

20. Smartt, H. B., Stewart, J. A., and Einerson, C. J. 1985. Paper presented at the 66th Annual AWS Convention, Las Vegas, Nev.

21. Khan, P. A. A., and DebRoy, T. 1985. Adsorption of CO_2 laser beam by AISI 4340 steel. *Metall. Trans.* Vol. 16B, p. 853.

22. Gogiberidze, Yu. M., Dzhincharadze, T. I., and Mikiashvili, Sh. M., 1968. *Soobshchi Akad. Nauk Gruz.* SSR (Bulletin of the Academy of Sciences of the Georgian SSR), Vol. 49, p. 415.

23. Paul, A., and DebRoy, T. 1988. Free surface flow and heat transfer in conduction mode laser welding. *Metallurgical Transactions* 19B, pp. 851-858.

24. Korpela, S. A., Ramanan, N., Tsai, C. L., and Lee, J. Y. 1988. Weld pool fluid mechanics and heat transfer in stationary welds. EWI research report, MR8810.

25. Katayama, S., and Matsunawa, A. 1984. Solidification microstructures of laser welded stainless steels. *Proc. of ICALEO 84.* Vol. 44. p. 60.

26. David, S. A., Vitek, J. M., and Hebble, T. L. 1987. Effect of rapid solidification on stainless steel weld metal microstructures and its implications on the Schaeffler diagram. *Welding Journal* 66(10):289-s.

27. Zacharia, T., David, S. A., Vitek, J. M., and DebRoy, T. 1989. Heat transfer during Nd:YAG pulsed laser welding and its effect on solidification structure of austenitic stainless steels. *Metallurgical Transactions* 20A, pp. 1125-1138.